SUPPORTING ONLINE MATERIAL

SPH method and analysis

Hydrodynamical models of giant impacts have typically used smooth particle hydrodynamics, or SPH (1-3, 15). SPH represents matter as particles that are tracked with time with a Lagrangian treatment. SPH is a computationally efficient method for modeling large impacts, because the code's numerical resolution follows the evolution of the colliding material as it disperses through a large total volume of space.

In SPH, colliding objects are described by a large number of spherically symmetric particles, each of which represents a quantity of mass of a given composition. The 3-D spatial distribution of each particle is defined with a density weighting function, known as the kernel, and a characteristic radius, known as the smoothing length, h. The functional form of the kernel does not change during a simulation, but the smoothing length of each particle is varied so as to maintain overlap with a desired number of other particles (typically a few tens), which allows low-density regions to be smoothly resolved, although with coarse spatial resolution.

In the version of SPH used here [a direct descendant of that of W. Benz used in (15)], the evolution of each particle's position, velocity, internal energy and density are evolved due to gravity, pressure forces, and shock dissipation. Material strength is neglected. A tree code is used for the gravity and nearest neighbor calculations, and the code is parallelized; each of the impact simulations reported here used 300,000 SPH particles and required about three days on an eight node machine. A detailed description of the SPH method is available in Benz (26), Section 6; the code here implements parameters as described in Appendix A of (2), including a beta spline kernel, variable smoothing lengths determined by a requirement

of a minimum of 40 and a maximum of 100 neighbor particles for each particle, and an artificial viscosity for converging particles with coefficients of $\alpha = 1.5$ and $\beta = 3.0$ for the bulk and von Neumann-Richtmyer terms [eqn. 6.2.15 in (26)], respectively.

The colliding objects are assumed to be differentiated, with each containing 30% iron and 70% mantle (dunite/forsterite) by mass, and are generated initially as a sphere of uniformly spaced SPH particles. The surface temperatures of both the impactor and the target are initially set to ~ 2000 K, with temperatures increasing along an adiabat with increasing depth as in (2). The objects are then simulated in isolation for about 10 hours, allowing them to settle to a hydrostatically equilibrated state prior to the collision.

The equation of state relates a particle's specific internal energy and local density to pressure at each time step. Our simulations use the semi-analytic equation of state known as ANEOS (17). In ANEOS, thermodynamic quantities are derived from the Helmholtz free energy, *F*, described as a sum of three components: a zero-temperature free energy, a nuclear component, and an electronic ionization term. The nuclear component is determined via an interpolation function that approximates a crystalline Debye solid at low temperatures and an ideal gas at high temperatures. A detailed description of the ANEOS method is contained in (17) and (27). ANEOS computes temperature as well as the mass fraction contained in each phase for mixed phase states. In SPH, each particle represents a single material, and mixed phase states (e.g., a two-phase vapor and melt) are described by treating the different phases as separate components that are in temperature and pressure equilibrium.

The classic ANEOS equation of state (17) treats vapor as monatomic, which requires a higher energy and entropy than molecular vapor. As a result, the original ANEOS underestimates vapor production for substances that form molecular species, including

mantle rock. Melosh (18) improved ANEOS to treat molecular vapor, considering one type of diatomic (or alternatively, triatomic) molecule as representative of a given material's vapor. Our SPH simulations consider dunite/forsterite mantles (with M-ANEOS parameters provided by E. Pierazzo and H. J. Melosh) and iron ANEOS cores, as in (2-3). These parameters are provided in Table S1.

We use an iterative procedure (1-3) to determine whether material is in the planet, in bound orbit around the planet, or escaping. An initial guess is made for the planet's size and therefore its mass (M_P) assuming a mean planet density comparable to that of the Earth. For each bound particle that is outside the planet, we compute an equivalent circular orbit semi-major axis, a_{eq}, defined by setting $\sqrt{GM_P a_{eq}}$ equal to the particle's specific angular momentum normal to the equatorial plane of the planet. The equivalent circular orbit is representative of that to which the mass represented by a particle would settle after undergoing mutual collisions, which rapidly damp orbital eccentricities and inclinations but transport angular momentum much more slowly. Those particles/cells with a_{eq} greater than the equatorial radius of the planet are defined as being "in the disk", and those that are energetically unbound as escaping. The mass of the planet is then recomputed as the total mass minus the mass of the disk and the mass of escaping particles, and the process is repeated until convergence is achieved on M_P. Given the calculated disk mass, M_D, and angular momentum, L_D, we use eqn. (1) from the main text to estimate the mass of the moon, M_M, that would later form from the disk assuming that $M_{esc} = 0$.

Impact simulation data

Figure S1 is comparable to Figure 2 in the main text, only here we show results for smaller impactors having $\gamma = 0.2$, which is the impactor size advocated by (14). The disks

that are massive enough to produce the Moon (i.e., with $M_M/M_P > 0.012$) have somewhat poorer compositional agreement with the final planet (with a minimum $|\delta f_T|$ value of 34%) than those produced by impacts with $\gamma = 0.3$ (minimum $|\delta f_T|$ value of 17%), and much poorer compositional agreement than those produced by impacts with $\gamma = 0.4$ and 0.45 (minimum $|\delta f_T|$ values of 6.6% and 0.3%, respectively).

How common are giant impacts with $\gamma \geq 0.4$ during the end stages of terrestrial planet accretion? Agnor et al. (22) considered between 20 and 50 initial planetary embryos in their accretion simulations, and provided a detailed analysis of impactor statistics. They found (their Table III) that the ratio of the mass of the largest impactor to collide with a planet (M_{lgst}) to the final planet's mass (M_P) is $\left\langle M_{lgst} / M_P \right\rangle = 0.32 \pm 0.08$ for planets with $M_P > 0.5M_\oplus$. Specifically, of the 20 planets having $M_P > 0.5M_\oplus$ at the end of the Agnor et al. simulations, four experienced a final large impact with $\gamma \geq 0.4$ or greater, or 20%. O'Brien et al. (23) considered 25 initial embryos together with 1000 smaller planetesimals and found that the mass of the final large impactor ranges from 0.1 to $0.4M_\oplus$ for planets with final masses $M_P > 0.5\ M_\oplus$. Because they did not provide the planet mass for each impactor mass, it is not possible to determine the distribution of γ from their data. Raymond et al. (28) consider about 90 initial embryos together with 1000 to 2000 planetesimals. Their Figure 5 details the mass growth histories of five planets with final masses $> 0.5M_\oplus$. Of these five planets, one experiences a final giant impact with $\gamma = 0.46$. Morishima et al. (29) consider 2000 initial planetary embryos, and include interactions of the embryos with a nebular gas disk. Their Figures 4 and 7 feature the mass growth histories of three planets with final masses $> 0.5M_\oplus$; from these figures, I estimate that two of the three planets experience a last

large impact with approximately $\gamma \geq 0.4$. Thus giant impacts between comparably sized bodies do occur, particularly towards the end stages of terrestrial accretion. Based on this rather limited number of cases, the probability of a late $\gamma \geq 0.4$ impact for a planet that grows to $M_P > 0.5\ M_\oplus$ appears to be roughly 20%.

Tables S2 through S5 provide data from all of the impact simulations. Columns show the run number, total impact angular momentum (L_T) in units of L_{EM} (3.5×10^{41} g cm^2 s^{-1}), the impact velocity scaled to the mutual escape velocity of the colliding objects (v_{imp}/v_{esc}), the scaled impact parameter (b), the disk mass in lunar masses (M_D/M_L), the disk angular momentum (L_D) in units of L_{EM}, the escaping mass scaled to the total mass (M_{esc}/M_T), the escaping angular momentum in units of L_{EM} in the center-of-mass frame of all of the material (L_{esc}/L_{EM}), the bound final angular momentum in units of L_{EM} in the center-of-mass frame of the bound material (L_F/L_{EM}), the fraction of the disk mass in iron (M_{Fe}/M_D), the predicted mass of the Moon (from eqn. 1 in the main text) in lunar masses (M_M/M_L), the predicted mass of the Moon scaled to the mass of the final planet (M_M/M_P), and the percentage compositional deviation of the disk from the final planet (δf_T), as computed from eqn. 2 in the main text).

All simulations were continued for 27 hours of simulated time. Cases indicating "binary" had a very large object on a bound but high-eccentricity orbit that would re-impact the planet on a timescale longer than that simulated. All runs considered non-rotating targets and impactors, with the exception of run 60* in Table S5, which considered a target with a 3 hour day whose pre-impact spin axis was anti-aligned to the angular momentum vector of the impact. "Successful" cases shown in Table 1 in the main text – defined as those with $M_M/M_P > 0.012$ and $|\delta f_T| \leq 15\%$ —are indicated in bold face in Tables S4 and S5.

Estimating disk-planet similarities needed to explain Earth-Moon compositions

Based on the estimates of (9), we assume that a typical large impactor during the late stages of terrestrial planet accretion had a compositional difference relative to that of the final planet that is comparable to the compositional difference between Earth and Mars. We adopt the epsilon notation, in which ε is the compositional deviation in parts per 10,000 from the terrestrial value, and set $\varepsilon_{\oplus} = 0$. We assume the deviation in the impactor's composition from that of the Earth (ε_{imp}) is comparable in magnitude to that of Mars (ε_{Mars}) and leave the target's composition, ε_{tar}, as a variable. By simple mass balance the silicate compositions of the resulting planet (ε_P) and its moon (ε_M) are

$$\begin{aligned} \varepsilon_P &= \varepsilon_{tar} F_{P,tar} + \varepsilon_{imp}(1 - F_{P,tar}) \\ \varepsilon_M &= \varepsilon_{tar} F_{D,tar} + \varepsilon_{imp}(1 - F_{D,tar}) \end{aligned}, \qquad \text{(S1)}$$

where $F_{P,tar}$ is the mass fraction of the silicate planet that originated from the target, and $F_{D,tar}$ is the mass fraction of the silicate disk that originated from the target (as in eqn. 2 in the main paper). Eqn. (S1) assumes that the Moon's final composition will be equal to that of the initial disk. We set $\varepsilon_P = \varepsilon_{\oplus} = 0$ and solve for ε_M,

$$\varepsilon_M = -\varepsilon_{imp}\left(\frac{F_{D,tar}}{F_{P,tar}} - 1\right) = -\varepsilon_{imp}\left(\frac{\delta f_T}{100}\right). \qquad \text{(S2)}$$

For an impactor with $\varepsilon_{imp} \sim |\varepsilon_{Mars}|$, one can then solve for the percentage δf_T deviation needed to achieve an observed deviation of the Moon from the Earth for a given element. This overall approach is motivated by that taken by (21).

For oxygen, the deviation of the Moon's composition from that of the Earth is $|\varepsilon_M(\text{oxygen})| < 0.05$ (4, 9), while Mars' deviation from the Earth is

$|\varepsilon_{Mars}(\text{oxygen})| \sim 3.2 \pm 0.13$ (9, 30), implying from eqn. (S2) that $|\delta f_T| < 1.6\%$ is required. This is broadly similar to the $|\delta f_T| < 5\%$ requirement for oxygen found by (21).

For titanium, recent work (6) finds $\varepsilon_M(\text{titanium}) = -0.03 \pm 0.04$. The titanium composition of Mars has recently reported values of $\varepsilon_{Mars}(\text{titanium}) = -0.77 \pm 0.10$, -0.30 ± 0.17, and -0.36 ± 0.17 (31). Using limiting values of $\varepsilon_M(\text{titanium}) = -0.07$ and $\varepsilon_{Mars}(\text{titanium}) = -0.67$ (the lower end of the range in the first measurement listed above, which used a similar instrument as the Zhang et al. (6) study), eqn. (S2) implies that $|\delta f_T| < 10\%$ could provide agreement with the Earth-Moon titanium similarities. However there is considerable uncertainty in this value given, in particular, the wide scatter and large uncertainties in the titanium values for Mars, which we use as a proxy for our impactor composition. For chromium, Mars samples appear to exhibit a characteristic $\varepsilon_{Mars}(\text{chromium}) \sim 0.24$ (32), while a lunar sample (5) has $\varepsilon_M = 0.0 \pm 0.1$, implying that $|\delta f_T| < 42\%$ could provide agreement with the Earth-Moon similarities in chromium, comparable to the $|\delta f_T| < 45\%$ value quoted in (21).

Although oxygen provides the most stringent constraints on $|\delta f_T|$ based on the calculations above, we note that the lunar values for titanium and chromium are also consistent within their uncertainties with $\varepsilon_M \approx 0$ for both elements, implying that an $|\delta f_T|$ value low enough to satisfy the oxygen constraint would still be consistent with those elements as well.

There is in addition uncertainty due to the likely spread of impactor compositions. Pahlevan and Stevenson (9) analyze 53 impacts from one of Chambers' (10) terrestrial

accretion simulations, and provide a histogram (their Figure 2) of the resulting deviation of impactor oxygen compositions from those of the final planets ($|\Delta^{17}O_{imp} - \Delta^{17}O_{planet}|$), assuming a linear variation in oxygen composition with heliocentric distance calibrated so that the third and fourth final planets from the Sun have the compositions of Earth and Mars, respectively. Their histogram implies a distribution of impactor compositions $|\Delta^{17}O_{imp} - \Delta^{17}O_{planet}| = 0.17 \pm 0.13$‰ (equivalent to a difference of 1.7 ± 1.3 in epsilon units). Our constraints on $|\delta f_T|$ above assume a Mars-composition impactor, which corresponds to the upper end of this distribution. The lower end of the distribution implies an impactor-to-planet compositional difference that is about 1/8th that of the Earth-Mars difference. Setting $\varepsilon_{imp}(\text{oxygen}) \sim |\varepsilon_{Mars}(\text{oxygen})|/8$ with $|\varepsilon_M(\text{oxygen})| = 0.05$ in eqn. (S2) gives a limiting value of $|\delta f_T| < 13\%$ for oxygen including likely variation in impactor composition.

The silicate Earth and the Moon also share similar tungsten (W) and silicon compositions, both of which are affected by core formation processes. Hafnium ^{182}Hf decays to ^{182}Wwith a half-life of $t_{1/2} = 9$ Myr; hafnium is lithophile ("silicate-liking"), while tungsten is siderophile ("iron-liking", or tending to enter metallic phases). During core formation, whatever tungsten is present in the mantle (including radiogenic ^{182}W as well as non-radiogenic W-isotopes, e.g. ^{184}W) will tend to be segregated into the core, while hafnium will remain in the mantle, so that the mantle of a differentiated object will have a Hf/W ratio larger than that of chondritic meteorites. If core formation occurs on a timescale $\leq 5t_{1/2} \sim 50$ Myr, a planet's mantle will contain excess ^{182}W (relative, e.g., to the abundance of ^{184}W) produced by decay of ^{182}Hf after core formation ends compared to chondritic values. The Hf/W and ^{182}W/^{184}W composition of a planet's mantle then reflect the degree

and timing of its integrated core formation process.

The silicate Earth and the Moon have essentially identical $^{182}W/^{184}W$ ratios, with $\varepsilon_M^{182}(\text{tungsten}) = 0.09 \pm 0.10$ (2 s.e.m.) and $\varepsilon_\oplus^{182}(\text{tungsten}) = 0$, and somewhat different Hf/W ratios (33). The $^{182}W/^{184}W$ similarity would be consistent with the proposed impact scenario if 1) the resulting silicate Earth and Moon contain approximately the same proportion of target vs. impactor material (comparable to the requirements from O, Ti, and Cr discussed above), and 2) mixing and equilibration between the protoearth's mantle and the iron cores of the impactor and the target did not substantially alter the $^{182}W/^{184}W$ ratio of the Earth's mantle relative to that of the Moon as the cores merge to form the final Earth's core.

Limited equilibration appears probable, because if the large cores of the target and impactor merge on the short timescale of the impact, they are unlikely to efficiently emulsify to the small sizes (= centimeter scale) needed for rapid equilibration with the surrounding mantle (34). Dahl and Stevenson (35) find that the degree of equilibration expected for an iron core descending through a mantle decreases as the core size increases, and estimate that < 1 weight percent of a 1000-km radius core would equilibrate with the protoearth's mantle. The cores in the impacts here are larger still – on the order of 2500-km in radius – and so would be expected to equilibrate with the protoearth's mantle to an even lesser degree. Further, if the Moon-forming impact occurs late at ≥ 50 Myr (as suggested by, e.g., [33]), metal-silicate equilibration may have a reduced ability to alter the $^{182}W/^{184}W$ ratio of the Earth compared to that of the Moon.

Figure S2 shows the behavior of the core material from the simulation shown in Figure 1 of the main paper. It is important to note several limitations of the SPH method

when interpreting this figure: first, each SPH particle resolves a quite coarse scale of ~ 100-km, and second, individual high-temperature iron particles may artificially "float" when surrounded by lower density silicate particles because the SPH method interpolates over the properties of the nearest neighbor particles to determine each particle's density (2). Nevertheless, the overall behavior shows that merger of the two cores occurs in < 10 hrs.

The Earth and Moon also have very similar Si isotope compositions ($\delta^{30}_{M}(\text{silicon}) = -0.31 \pm 0.03$‰ and $\delta^{30}_{\oplus}(\text{silicon}) = -0.38 \pm 0.06$‰ [36]), which are distinct from those of meteorites or Mars. A likely explanation for Earth's silicon composition is that silicon was incorporated into its core through what is believed to be a high-pressure, high-temperature effect that becomes important once a planet reaches ~ 0.15 Earth masses (see 36 and references therein). The impact scenario here would be consistent with the identical Si isotopic compositions of the Earth and Moon if these compositions were inherited from the mantles of the impactor and target (themselves each massive enough to have incorporated silicon into their cores), which were then mixed in approximately equal proportions in the Earth and Moon. Substantial additional fractionation of Si into the cores of the impactor and target as they descend through the protoearth's mantle would need to be avoided to keep the Earth's silicon composition from diverging from that of the Moon. This may be likely given the limited degree of intimate mixing between the silicate and metal expected for such large cores, as discussed above.

Additional References

26. W. Benz. In "*Late stages of stellar evolution: Computational methods in hydrodynamics*," Springer-Verlag, Berlin, 258 (1989).

27. S. L. Thompson. *Sandia Rep. SAND89-2951*, Sandia Nat. Labs (1990).

28. S. N. Raymond, D. P. O'Brien, A. Morbidelli, N. A. Kaib. *Icarus* **203**, 644 (2009).

29. R. Morishima, J. Stadel, B. Moore. *Icarus* **207**, 517 (2010).

30. A. Franchi, I. P. Wright, A. S. Sexton, T. Pillinger. *Meteorit. Planet. Sci.* **34**, 657 (1999).

31. A. Trinquier, T. Elliott, D. Ulfbeck, C. Coath, A. N. Krot, M. Bizzarro, *Science* **324**, 375 (2009).

32. A. Shukolyukov, G. W. Lugmair, *Space Sci. Rev*. **92**, 225 (2000).

33. M. Touboul, T. Kleine, B. Bourdon, H. Palme, R. Wieler. *Nature* **450**, 1206 (2007).

34. D. C. Rubie, H. J. Melosh, J. E. Reid, C. Liebske, K. Righter. *Earth Plan. Sci. Lett.* **205**, 239 (2003).

35. T. W. Dahl, D. J. Stevenson. *Earth Planet. Sci. Lett.* **295**, 177 (2010).

36. R. B. Georg, A. N. Halliday, E. A. Schauble, B. C. Reynolds. *Nature* **447**, 1102 (2007).

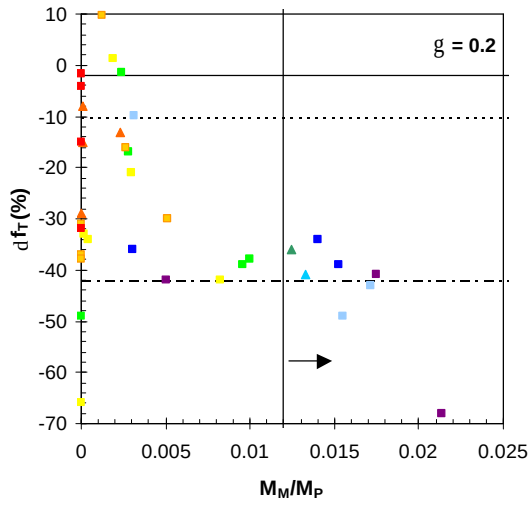

Figure S1: Results of SPH simulations of $\gamma = 0.2$ impacts. Color indicates impact velocity relative to the escape velocity as in Figure 2 in the main text, although here there are two additional values: $v_{imp}/v_{esc} = 1.25$ indicated by the azure blue triangle, and $v_{imp}/v_{esc} = 1.35$ indicated by the green triangle. Plotted are the relative difference in the final disk-planet compositions (δf_T) vs. the predicted mass of the moon that would accrete from each disk divided by the planet's mass. An appropriately massive moon requires $(M_M/M_P) \geq 0.012$, or to the right of the vertical line. Horizontal lines indicate estimated requirements for meeting oxygen (solid), titanium (dotted) and chromium (dot-dashed) constraints assuming a Mars-composition impactor.

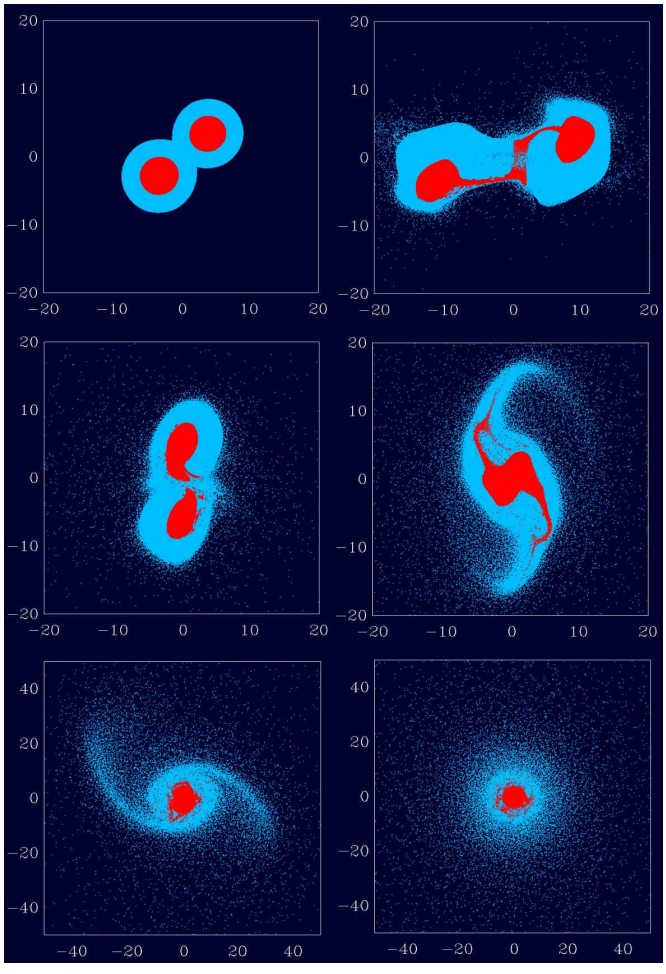

Figure S2: Behavior of iron (red) vs. silicate (blue) material in the impact simulation shown in Figure 1 of the main text. Here all iron particles are plotted on top of the silicate particles for clarity. Distances are in units of 10^3 km. Panels are shown at the same times as those in Figure 1.

Table S1: Dunite/Forsterite (Mg_2SiO_4) M-ANEOS and Iron ANEOS parameters used in the SPH simulations here and in (2-3); see (15, 17-18, 27) for details. Variables related to molecular vapor treatment for dunite indicated with superscript "m".

Variable	Dunite	Iron	Description
V1	3	1	Number of elements in material
V2	4	4	EOS Type; 4 = Solid-gas with electronic terms and detailed treatment of liquid/vapor region
V3	3.32	7.85	Reference density (g cm^{-3})
V4	0	0	Reference temperature (for 0, defaults to 298 K).
V5	0.	0.	Reference pressure (normally 0)
V6	−6.6e5	1.45e12	If negative sign included, value is S_o (in cm s^{-1}) from the shock-particle velocity relation, $u_s=S_o+S_1u_p$. Positive values correspond to the reference bulk modulus (dyne cm^2)
V7	0.82	1.690	Reference Gruneisen coefficient
V8	0.057	−0.04	Reference Debye temperature (eV); if < 0, uses full treatment of Debye functions; if > 0, uses high temperature approximation
V9	0.86	0	S_1 from shock-particle velocity relation
V10	2.	2.	Three times the limiting value of the Gruneisen coefficient for large compression (usually 0 or 2)
V11	1.3e11	8.2e10	Zero-temperature separation energy (erg g^{-1}), or vaporization energy for molecular species
V12	0.19	0.15588	Melting temperature at zero pressure (eV)
V13	0	0	parameter c_{53}, for low density modification to move the critical point (if 0, not used)
V14	0	0	parameter c_{54}, for low density modification to move the critical point (if 0, not used)
V15	0.	0	H_0, thermal conductivity parameter; 0 if thermal conduction not included
V16	0	0	c_{41},thermal conductivity parameter; 0 if not included
V17	0.	0.	Lowest allowed solid density; if 0, defaults to 0.9 times reference density
V18	4.65	0.	D1, Density at onset of high pressure phase transition (hppt)
V19	4.9	0.	D2, Density at completion of hppt
V20	6.6e11	0.	Pressure at center of hppt (dyne cm^{-2})
V21	3.5e12	0.	$dP/d\eta$ at end of hppt (dyne cm^{-2})
V22	1.3e13	0.	$d^2P/d\eta^2$ (dyne cm^{-2})
V23	0.	2.471e9	Heat of fusion (not included if 0)
V24	0.	0.955	Liquid/solid density at the melting point (0 for no melt phase)

V25-V32			Not used.
V33	1	0	Flag for ionization model. 0=Saha; 1=Thomas-Fermi
V34	0.	0.	E_{shift}, energy shift for reactive chemistry modeling.
V35	0.	0.	S_{shift}, entropy shift for reactive chemistry modeling.
V36[m]	2	N/A	Number of atoms in molecular clusters
V37[m]	1.5e–8	N/A	Length of molecular bond (cm)
V38[m]	8.0	N/A	E_{bind} (eV)
V39[m]	0	N/A	Interior degrees of freedom
V40	1	0	Flags use of Lennard-Jones (1) or standard ANEOS cold potential (0)
V41	1.25	0	Cold pressure exponent ("a" in ref. (18), eq.4)
Elements in material	3	1	Equal to V1
Element; atomic number, fraction	O; 8, 0.571	Fe; 26, 1	
Element; atomic number, fraction	Mg; 12, 0.286		
Element; atomic number, fraction	Si; 14, 0.143		

Table S2. Impacts with $\gamma = 0.2$ and $M_T = 1.038 M_\oplus$

run	L_T/L_{EM}	v_{imp}/v_{esc}	b	M_D/M_L	L_D/L_{EM}	M_{esc}/M_T	L_{esc}/L_{EM}	L_F/L_{EM}	M_{Fe}/M_D	M_M/M_L	M_M/M_P	δf_T (%)
5	1.44	1.4	0.4	0.44	0.064	0.044	0.37	1.06	0.005	0.19	2.37E-03	-1.5
6	1.65	1.6	0.4	0.62	0.084	0.075	0.62	1.02	0.058	0.23	2.97E-03	-21
7	1.86	1.8	0.4	0.61	0.094	0.11	0.987	0.89	1.8	0.38	5.10E-03	-30
8	2.06	2	0.4	0.198	0.019	0.22	1.84	0.29	0.037	0.008	1.22E-04	-8
9	1.63	1.4	0.45	0.65	0.088	0.051	0.48	1.13	0.065	0.22	2.77E-03	-17
10	1.86	1.6	0.45	1.02	0.16	0.082	0.83	1.02	0.2	0.63	8.24E-03	-42
11	2.09	1.8	0.45	binary								
12	2.32	2	0.45	0.21	0.016	0.25	2.044	0.25	0.036	0	0.00E+00	-29
13	1.55	1.2	0.5	0.6	0.087	0.029	0.29	1.26	0.04	0.25	3.07E-03	-36
14	1.81	1.4	0.5	1.32	0.21	0.059	0.7	1.16	0.095	0.78	9.99E-03	-38
15	2.07	1.6	0.5	binary								
16	2.33	1.8	0.5	0.22	0.017	0.19	1.82	0.34	0.04	0	0.00E+00	-38
17	1.71	1.2	0.55	1.79	0.29	0.031	0.35	1.36	0.061	1.12	1.40E-02	-34
18	1.99	1.4	0.55	0.94	0.164	0.061	0.82	1.22	0.095	0.75	9.58E-03	-39
19	2.28	1.6	0.55	0.161	0.017	0.17	1.69	0.4	0.04	0.014	2.00E-04	-33
20	2.56	1.8	0.55	0.15	0.011	0.28	2.34	0.24	0.053	0	0.00E+00	-37
21	1.86	1.2	0.6	1.55	0.274	0.037	0.45	1.41	0.03	1.22	1.53E-02	-39
22	2.17	1.4	0.6	0.22	0.02	0.15	1.55	0.46	0.012	0	0.00E+00	-49
23	2.48	1.6	0.6	0.12	0.014	0.18	1.84	0.36	0.046	0.026	3.76E-04	-34
24	2.79	1.8	0.6	0.16	0.014	0.3	2.48	0.22	0.11	0.002	3.39E-05	-31
25	1.45	1.6	0.35	0.4	0.054	0.067	0.49	0.93	0.022	0.15	1.91E-03	1.4
26	1.63	1.8	0.35	0.53	0.071	0.098	0.7	0.91	0.084	0.2	2.65E-03	-16
27	1.81	2	0.35	binary								
28	2.26	2.5	0.35	0.28	0.017	0.31	1.94	0.16	0.23	0	0.00E+00	-15
30	1.39	1.8	0.3	0.34	0.043	0.091	0.54	0.82	0.007	0.097	1.27E-03	9.6
31	1.55	2	0.3	0.48	0.061	0.13	0.81	0.75	0.063	0.17	2.33E-03	-13
32	1.94	2.5	0.3	0.35	0.012	0.37	1.88	0.15	0.28	0	0.00E+00	-32
34	2.58	2.5	0.4	0.25	0.019	0.29	2.06	0.17	0.08	0	0.00E+00	-4.1
35	1.94	1.25	0.6	1.48	0.25	0.045	0.59	1.35	0.11	1.05	1.33E-02	-41
36	2.02	1.3	0.6	2.45	0.361	0.048	0.71	1.37	0.1	1.21	1.55E-02	-49
37	1.85	1.3	0.55	1.57	0.286	0.048	0.57	1.29	0.082	1.35	1.71E-02	-43
38	1.51	1.3	0.45	0.6	0.086	0.037	0.34	1.16	0.015	0.25	3.10E-03	-9.8
39	2.91	2.5	0.45	0.23	0.019	0.31	2.46	0.16	0.1	0.001	1.72E-05	-1.6
40	2.59	2	0.5	0.18	0.016	0.29	2.33	0.28	0.057	0.006	1.00E-04	-15
41	1.7	1.1	0.6	1.91	0.332	0.023	0.26	1.43	0.042	1.41	1.75E-02	-41
42	1.56	1.1	0.55	0.81	0.124	0.021	0.21	1.35	0.051	0.41	5.01E-03	-42
43	1.92	1.35	0.55	1.16	0.21	0.055	0.66	1.27	0.086	0.98	1.25E-02	-36
44	2.09	1.35	0.6	binary								
45	1.84	1.1	0.65	2.42	0.42	0.011	0.15	1.69	0.035	1.73	2.13E-02	-68

Table S3. Impacts with $\gamma = 0.3$ and $M_T = 1.038M_\oplus$

run	L_T/L_{EM}	v_{imp}/v_{esc}	b	M_D/M_L	L_D/L_{EM}	M_{esc}/M_T	L_{esc}/L_{EM}	L_F/L_{EM}	M_{Fe}/M_D	M_M/M_L	M_M/M_P	δf_T (%)
1	1.68	1.6	0.3	0.63	0.086	0.087	0.46	1.2	0.012	0.25	3.27E-03	16
2	1.89	1.8	0.3	0.58	0.075	0.143	0.85	1.06	0.016	0.23	3.21E-03	4.7
3	2.1	2	0.3	0.54	0.036	0.346	1.98	0.28	0.037	0	0.00E+00	-28
4	2.3	2.2	0.3	0.26	0.016	0.4	1.84	0.2	0.058	0	0.00E+00	
5	1.71	1.4	0.35	0.67	0.094	0.054	0.32	1.38	0.026	0.27	3.41E-03	-17
5	1.96	1.6	0.35	0.73	0.1	0.095	0.64	1.3	0.034	0.31	4.10E-03	-0.3
7	2.2	1.8	0.35	binary								
8	2.44	2	0.35	0.32	22	0.363	1.972	0.202	0.042	0	0.00E+00	-9
9	1.67	1.2	0.4	0.8	0.11	0.025	0.15	1.52	0.064	0.28	3.44E-03	-36
10	1.81	1.3	0.4	1.03	0.144	0.039	0.26	1.55	0.074	0.4	5.00E-03	-35
11	1.96	1.4	0.4	1.01	0.141	0.059	0.41	1.54	0.027	0.41	5.23E-03	-20
12	2.24	1.6	0.4	0.87	0.134	0.102	0.88	1.38	0.016	0.53	7.07E-03	-17
13	2.51	1.8	0.4	0.2	0.012	0.38	2.28	0.19	0.027	0	0.00E+00	-15
14	1.89	1.2	0.45	1.7	0.248	0.021	0.14	1.75	0.055	0.74	9.15E-03	-43
15	2.04	1.3	0.45	1.74	0.243	0.043	0.3	1.73	0.018	0.7	8.86E-03	-43
16	2.2	1.4	0.45	1.87	0.278	0.06	0.51	1.68	0.063	0.96	1.24E-02	-17
17	2.51	1.6	0.45	binary								
18	1.92	1.1	0.5	1.69	0.263	0.0094	0.04	1.88	0.0037	0.89	1.09E-02	-28
19	1.09	1.2	0.5	3.12	0.762	0.019	-0.9	1.99	0.024	1.49	1.87E-02	-41
20	2.27	1.3	0.5	2.4	0.373	0.044	0.41	1.86	0.058	1.39	1.78E-02	-33
21	2.44	1.4	0.5	2.25	0.367	0.061	0.64	1.82	0.057	1.52	1.97E-02	-33
22	2.11	1.1	0.55	2.87	0.473	0.01	0.06	2.05	0.03	1.84	2.28E-02	-53
23	2.3	1.2	0.55	2.96	0.48	0.016	0.14	2.16	0.056	1.85	2.31E-02	-53
24	2.49	1.3	0.55	4.35	0.797	0.022	0.16	2.33	0.036	3.82	4.89E-02	-67
25	2.69	1.4	0.55	6.36	0.38	0.18	1.68	0.7	0.32	0	0.00E+00	-66
26	2.3	1.1	0.6	3.65	0.607	0.008	0.06	2.24	0.062	2.44	3.05E-02	-52
27	2.51	1.2	0.6	3.79	0.7	0.013	0.12	2.39	0.029	3.3	4.15E-02	-45
28	2.72	1.3	0.6	binary								
29	2.94	1.4	0.6	0.045	0.004	0.28	1.987	0.287	0.006	0	0.00E+00	-35
30	1.4	1.6	0.6	0.31	0.037	0.081	0.33	1.05	0.006	0.07	9.06E-04	15
31	1.57	1.8	0.25	0.44	0.049	0.134	0.56	0.97	0.005	0.07	9.64E-04	23
32	1.75	2	0.25	0.53	0.06	0.202	0.907	0.849	0.02	0.14	2.10E-03	10
33	1.92	2.2	0.25	0.5	0.017	0.45	1.9	0.21	0.15	0	0.00E+00	-22

Table S4. Impacts with $\gamma = 0.4$ and $M_T = 1.038M_\oplus$

run	L_T/L_{EM}	v_{imp}/v_{esc}	b	M_D/M_L	L_D/L_{EM}	M_{esc}/M_T	L_{esc}/L_{EM}	L_F/L_{EM}	M_{Fe}/M_D	M_M/M_L	M_M/M_P	δf_T (%)
1	**2.41**	**1**	**0.6**	**2.94**	**0.512**	**0.010**	**0.09**	**2.32**	**0.008**	**2.17**	**2.69E-02**	**-9**
2	2.65	1.1	0.6	4.35	0.748	0.019	0.13	2.52	0.028	3.22	4.11E-02	-29
3	**2.21**	**1**	**0.55**	**1.74**	**0.289**	**0.007**	**0.03**	**2.18**	**0.018**	**1.1**	**1.34E-02**	**11**
4	**2.44**	**1.1**	**0.55**	**2.72**	**0.417**	**0.010**	**0.05**	**2.39**	**0.05**	**1.41**	**1.74E-02**	**-15**
5	2.66	1.2	0.55	4.15	0.644	0.023	0.24	2.42	0.025	2.37	3.03E-02	-21
6	**2.01**	**1**	**0.5**	**2.16**	**0.389**	**0.008**	**0.05**	**1.96**	**0.02**	**1.71**	**2.10E-02**	**13**
7	**2.21**	**1.1**	**0.5**	**1.93**	**0.302**	**0.010**	**0.04**	**2.17**	**0.053**	**1.05**	**1.29E-02**	**-6.6**
8	2.41	1.2	0.5	4.41	0.734	0.014	0.06	2.35	0.056	3.03	3.85E-02	-22
9	2.61	1.3	0.5	3.86	0.634	0.028	0.21	2.4	0.03	2.6	3.33E-02	-38
10	1.99	1.1	0.45	1.75	0.284	0.017	0.15	1.84	0.032	1.07	1.32E-02	-35
11	2.17	1.2	0.45	0.91	0.123	0.017	0.05	2.12	0.025	0.28	3.41E-03	-22
12	2.35	1.3	0.45	2.74	0.400	0.025	0.11	2.24	0.041	1.24	1.56E-02	-35
13	2.53	1.4	0.45	4.73	0.758	0.360	0.13	2.40	0.049	3.09	4.03E-02	-54
14	1.77	1.1	0.4	1.67	0.268	0.014	0.06	1.71	0.022	0.98	1.20E-02	-33
15	2.25	1.4	0.4	1.53	0.215	0.044	0.17	2.08	0.024	0.62	7.83E-03	-34
16	2.57	1.6	0.4	binary								
17	2.25	1.6	0.35	0.98	0.140	0.100	0.54	1.71	0.024	0.48	6.40E-03	3.8
18	2.82	1.4	0.5	binary								

Table S5. Impacts with $\gamma = 0.45$ and $M_T = 1.038M_\oplus$

run	L_T/L_{EM}	v_{imp}/v_{esc}	b	M_D/M_L	L_D/L_{EM}	M_{esc}/M_T	L_{esc}/L_{EM}	L_F/L_{EM}	M_{Fe}/M_D	M_M/M_L	M_M/M_P	δf_T (%)
1	1.45	1.4	0.25	0.22	0.021	0.057	0.11	1.34	0.001	0	0.00E+00	-8
2	1.66	1.6	0.25	0.45	0.059	0.11	0.3	1.36	0.009	0.15	2.01E-03	10
3	1.87	1.8	0.25	0.73	0.088	0.18	0.66	1.2	0.014	0.24	3.51E-03	9.9
4	2.07	2	0.25	1.06	0.112	0.25	1.13	0.93	0.072	0.24	3.86E-03	-1.4
5	1.74	1.4	0.3	0.332	0.042	0.051	0.1	1.64	0.002	0.077	9.65E-04	-14
6	1.99	1.6	0.3	0.478	0.069	0.1	0.36	1.62	0.01	0.242	3.21E-03	3.7
7	2.25	1.8	0.3	1.4	0.185	0.18	1	1.33	0.087	0.67	9.88E-03	23
9	1.89	1.3	0.35	0.37	0.05	0.029	0.04	1.85	0.009	0.12	1.47E-03	-9
10	2.03	1.4	0.35	0.245	0.034	0.042	0.1	1.93	0.007	0.094	1.17E-03	-46
11	**2.32**	**1.6**	**0.35**	**2.3**	**0.31**	**0.102**	**0.43**	**1.89**	**0.061**	**0.96**	**1.31E-02**	**-5**
14	**1.82**	**1.1**	**0.4**	**1.87**	**0.299**	**0.014**	**0.05**	**1.77**	**0.034**	**1.09**	**1.34E-02**	**-1**
15	1.99	1.2	0.4	1.82	0.261	0.02	0.05	1.94	0.015	0.75	9.27E-03	-12
16	2.16	1.3	0.4	0.38	0.05	0.024	0.04	2.12	0.021	0.1	1.22E-03	-15
17	**2.32**	**1.4**	**0.4**	**2.88**	**0.394**	**0.038**	**0.09**	**2.22**	**0.028**	**1.09**	**1.39E-02**	**-0.3**
18	2.64	1.6	0.4	binary								
20	2.05	1.1	0.45	2.03	0.342	0.013	0.05	2	0.013	1.36	1.67E-02	21
21	2.24	1.2	0.45	0.47	0.059	0.016	0.04	2.2	0.029	0.11	1.33E-03	-8
22	2.43	1.3	0.45	3.76	0.55	0.026	0.09	2.34	0.025	1.79	2.28E-02	-22
23	2.61	1.4	0.45	4.51	0.647	0.036	0.13	2.48	0.041	2.1	2.73E-02	-23
25	2.07	1	0.5	2.08	0.345	0.008	0.04	2.03	0.004	1.42	1.74E-02	37
26	2.28	1.1	0.5	2.02	0.298	0.012	0.04	2.24	0.008	0.91	1.12E-02	9
27	2.49	1.2	0.5	3.63	0.579	0.02	0.15	2.34	0.03	2.22	2.81E-02	-16
28	2.69	1.3	0.5	5	0.737	0.025	0.13	2.56	0.027	2.52	3.26E-02	-21
29	2.91	1.4	0.5	binary								
30	2.28	1	0.55	2.54	0.432	0.013	0.14	2.14	0.007	1.77	2.19E-02	26
31	**2.51**	**1.1**	**0.55**	**3.03**	**0.47**	**0.01**	**0.06**	**2.45**	**0.019**	**1.64**	**2.04E-02**	**-0.8**
32	**2.74**	**1.2**	**0.55**	**5.06**	**0.778**	**0.022**	**0.22**	**2.52**	**0.028**	**2.89**	**3.73E-02**	**-8**
33	2.97	1.3	0.55	0.345	0.062	0.01	0.04	2.93	0.017	0.263	3.16E-03	-11
35	**2.49**	**1**	**0.6**	**2.84**	**0.474**	**0.011**	**0.12**	**2.37**	**0.007**	**1.88**	**2.33E-02**	**-6**
37	2.99	1.2	0.6	5.98	1.01	0.02	0.15	2.84	0.01	4.43	5.77E-02	-17
38	3.24	1.3	0.6	binary								
39	**2.7**	**1**	**0.65**	**3.63**	**0.602**	**0.008**	**0.09**	**2.61**	**0.004**	**2.40**	**3.00E-02**	**-13**
40	**2.97**	**1.1**	**0.65**	**5.46**	**0.897**	**0.022**	**0.34**	**2.63**	**0.008**	**3.75**	**4.87E-02**	**-15**
41	3.24	1.2	0.65	binary								
43	**2.91**	**1**	**0.7**	**5.58**	**0.973**	**0.012**	**0.2**	**2.71**	**0.003**	**4.39**	**5.66E-02**	**-15**
44	3.19	1.1	0.7	6.89	1.17	0.016	0.22	2.97	0.001	5.23	6.87E-02	-35
60*	**2.23**	**1.2**	**0.55**	**2.39**	**0.367**	**0.017**	**0.08**	**2.15**	**0.053**	**1.26**	**1.56E-02**	**10**